ELSEVIER

Journal of Structural Geology 29 (2007) 819–836

JOURNAL OF STRUCTURAL GEOLOGY

www.elsevier.com/locate/jsg

The role of fluids in low temperature, fault-related deformation of quartz arenite

Allyson O'Kane, Charles M. Onasch*, John R. Farver

Department of Geology, Bowling Green State University, Bowling Green, OH 43403, USA

Received 30 June 2006; received in revised form 4 January 2007; accepted 4 January 2007
Available online 26 January 2007

Abstract

The microstructural and fluid histories in quartz arenite deformed in a regional-scale fault zone were investigated to determine the role of fluids in the selection of grain-scale deformation mechanisms. Using cathodoluminescence, fluid inclusion microthermometry, and stable isotope geochemistry of quartz cements, three chemically distinct, aqueous fluids were identified that affected the rock at different times during deformation. The earliest deformation microstructures are distributed cataclasites, which were cemented by reddish-brown luminescing quartz precipitated from an aqueous, $CaCl_2$ brine (Fluid I). Once cemented, brittle deformation continued, but localized along discrete shear surfaces, in narrow zones 20–1000 μm wide, and on discrete microfractures. Microveins associated with this phase were cemented with bluish-green luminescing quartz precipitated from an aqueous, $CaCl_2$ brine (Fluid II). Water, channelized along dissolution surfaces and in pervasive microfracture networks that formed at this time, promoted hydrolytic weakening and crystal-plastic deformation, especially near fluid pathways. Temperatures during deformation associated with Fluids I and II were 225–235 °C as determined from fluid inclusion data. In the later stages of deformation, an influx of iron-bearing aqueous fluid (Fluid III) greatly accelerated the rate of quartz dissolution and filled fractures, stylolites, and vugs with goethite. The progression of deformation mechanisms indicated by the microstructures and their relationship to the different fluids show that the selection of grain-scale deformation processes is affected not only by the presence of fluids, but also by their chemistry.
© 2007 Elsevier Ltd. All rights reserved.

Keywords: Fluids; Microstructures; Deformation mechanisms; Fault zone

1. Introduction

Deformation occurring in rocks at subgreenschist conditions (<300 °C) affects a significant volume of the Earth's crust. Under these conditions, fluids play an integral role in controlling grain-scale deformational processes through both mechanical and chemical effects (Carter et al., 1990). At temperatures less than ~150 °C, the effect of fluids is dominantly mechanical through fluid pressure, which reduces the effective normal stress (Hubbert and Rubey, 1959; Secor, 1965). As the fluid pressure increases in a stress regime in which differential stress is modest, Mode I fractures form through hydrofracturing where the fluid pressure equals or exceeds the minimum principal stress. The grain-scale expression of Mode I fractures includes open and healed microfractures (e.g., fluid inclusion planes and microveins) (Pollard and Aydin, 1988; Onasch, 1990; Laubach, 1997; Lespinasse, 1999; Blenkinsop, 2000; Laubach et al., 2004). At higher effective stresses, shear failure occurs and can trigger cataclasis, which can be an important process in the formation and subsequent evolution of a fault zone (Sibson, 1977; Lloyd and Knipe, 1992; Imber et al., 2001; Holdsworth, 2004). During cataclasis, high fluid pressure facilitates grain-boundary sliding and grain rotation, and if sufficiently high, leads to fluidization where clastic material is injected into dilated fractures (Sibson, 1977).

At temperatures above ~300 °C, chemical effects become important and are a function of fluid chemistry (Carter et al.,

* Corresponding author. Fax: +1 419 372 7205.
E-mail address: conasch@bgsu.edu (C.M. Onasch).

0191-8141/$ - see front matter © 2007 Elsevier Ltd. All rights reserved.
doi:10.1016/j.jsg.2007.01.003

1990; Post and Tullis, 1998; Wawrzyniec et al., 1999). In the case of aqueous fluids, processes such as diffusive mass transfer (Rutter, 1983; Groshong, 1988; Knipe, 1989), hydrolytic weakening (Griggs and Blacic, 1965; Paterson, 1989; Paterson and Luan, 1990; Kronenberg, 1994; Post et al., 1996), and stress corrosion (Atkinson, 1984) control deformation at the grain scale. Non-aqueous fluids, such as CO_2 and CH_4, however, promote brittle deformation in environments where a more ductile response would be expected (Selverstone et al., 2003; Selverstone, 2005; Cook et al., 2006).

At temperatures between 150 °C and 300 °C, both brittle and ductile deformation mechanisms can operate (Ashby, 1972), and the presence and composition of fluids may be the determining factor as to which one dominates. For example, in the lower portion of this temperature regime, brittle processes would be expected to dominate because the rate of dislocation creep is low (Hirth and Tullis, 1992). However, in the presence of aqueous fluids, hydrolytic weakening can reduce the flow stress to the point where significant dislocation-related microstructures develop (Carter et al., 1990; Kronenberg et al., 1990). In this transitional temperature regime, interactions between brittle and ductile processes may also be important. For example, microfracturing reduces the grain size and facilitates grain-scale fluid flow that enhances diffusive mass transport and mineral reactions (Den Brok and Spiers, 1991; Stewart et al., 2000; Imber et al., 2001; Jefferies et al., 2006).

Because fault zones are dilatant and act as conduits for channelized fluid flow (McCaig, 1989; Logan, 1991; Knipe, 1992; Caine et al., 1996; Sibson, 1996; Evans et al., 1997; Holdsworth, 2004), they are an ideal location in which to study the effects of fluids on grain-scale deformation. Alternations between brittle and ductile deformation recorded in many fault zones are commonly interpreted to be due to time-varying strain rates resulting from fluctuating pore fluid pressure or to the earthquake cycle (Sibson et al., 1988; Sibson, 1990, 2001; Cox et al., 2001; Boullier and Robert, 1992; Cox, 1995). However, variations in the amount of fluids or changes in fluid chemistry could also produce the same variations (Stewart et al., 2000; Imber et al., 2001; Holdsworth, 2004; Jefferies et al., 2006).

In order to better understand the models that have been developed to explain how fluids and fluid chemistry affect the macroscopic behavior of rocks, an investigation of grain-scale processes in an environment known to contain fluids is necessary. The purpose of our study is to describe the interplay between fluids and grain-scale deformational processes in low temperature, fault-related deformation of quartz-rich rocks, and show how water affected the selection of grain-scale deformational mechanisms, and hence, the macroscopic behavior of these rocks. Specifically, we have used transmitted and cathodoluminescence (CL) microscopy, fluid inclusion microthermometry, Fourier Transform Infrared (FTIR) spectroscopy, and stable isotope geochemistry to characterize the fluids present during the deformation of quartz arenite in a fault zone where temperatures were less than 250 °C, and to link them to the grain-scale deformational history.

2. Geologic setting

The samples for this study are from the Cove fault zone in the central Appalachian foreland thrust belt (Fig. 1). This Alleghanian thrust belt consists of a blind duplex of Cambro-Ordovician carbonates overlain by a roof sequence composed of Ordovician to Pennsylvanian clastic and carbonate rocks (Evans, 1989; Hatcher et al., 1989). The Cove fault, which post-dates most of the folding in the region, cuts the northwest limb of the Big Cove anticline in the roof sequence and juxtaposes Cambrian and younger rocks in the anticlinal core with Devonian and Mississippian clastics in the adjacent syncline to the west (R. Nickelsen, personal communication, 2003) (Fig. 1).

The target lithology for this study is the Lower Silurian Tuscarora Sandstone, a medium-grained, framework-supported quartz arenite. On the whole, the sandstone is well cemented with typically less than 5% porosity (Sibley and Blatt, 1976; Cotter, 1983; Houseknecht, 1988), but irregular bed-scale cement distribution can lead to local porosities of up to 10% (Heald and Anderegg, 1960; Ryder and Zagorski, 2003). In south-central Pennsylvania, the Tuscarora Sandstone was buried to a maximum depth of ~7 km and was deformed during the Alleghanian orogeny at temperatures between 150 °C and 250 °C (Epstein et al., 1977; Harris et al., 1978; Onasch and Dunne, 1993; Evans, personal communication, 2006). It is exposed continuously on the southeast limb, hinge, and a portion of the northwest limb of the Big Cove anticline (Fig. 1). The sandstone is also found in several isolated horses along the Cove fault just north of where it truncates the sandstone in the northwest limb (Fig. 1). These horses are believed to have been sheared from the footwall during displacement on the Cove fault. Samples for this study were collected from the northwest limb of the anticline, just south of where the fault truncates the Tuscarora Sandstone, and from two of the horses just north of this truncation (Fig. 1). Within the two horses, the preserved thickness of the Tuscarora Sandstone ranges between 15 and 30 m. Away from the Cove fault, it attains an average thickness of 100 m (Cotter, 1983).

The amount of mesoscopic deformation increases progressively from south to north. In the northwest limb near its truncation by the Cove fault (Fig. 1), conspicuous bedding defined by variations in grain size and/or the amount of impurities is cut by joints and faults with a spacing of 5–20 m and displacements of less than 1 m. In contrast, bedding in the northern horse (Fig. 1) has been nearly obliterated. The numerous planar and curved surfaces present are presumed to be faults based on the abundance of fractures and breccia (Fig. 2a). The lack of stratigraphic markers, however, prevents accurate determination of displacements. A number of the surfaces have depressions or open cavities up to several centimeters deep, spaced 1–2 m apart, which are commonly coated or filled with goethite (Fig. 2b). The southern horse is transitional in character between the northwest limb and the northern horse. Nowhere in any of the sample sites was the contact with the surrounding units exposed.

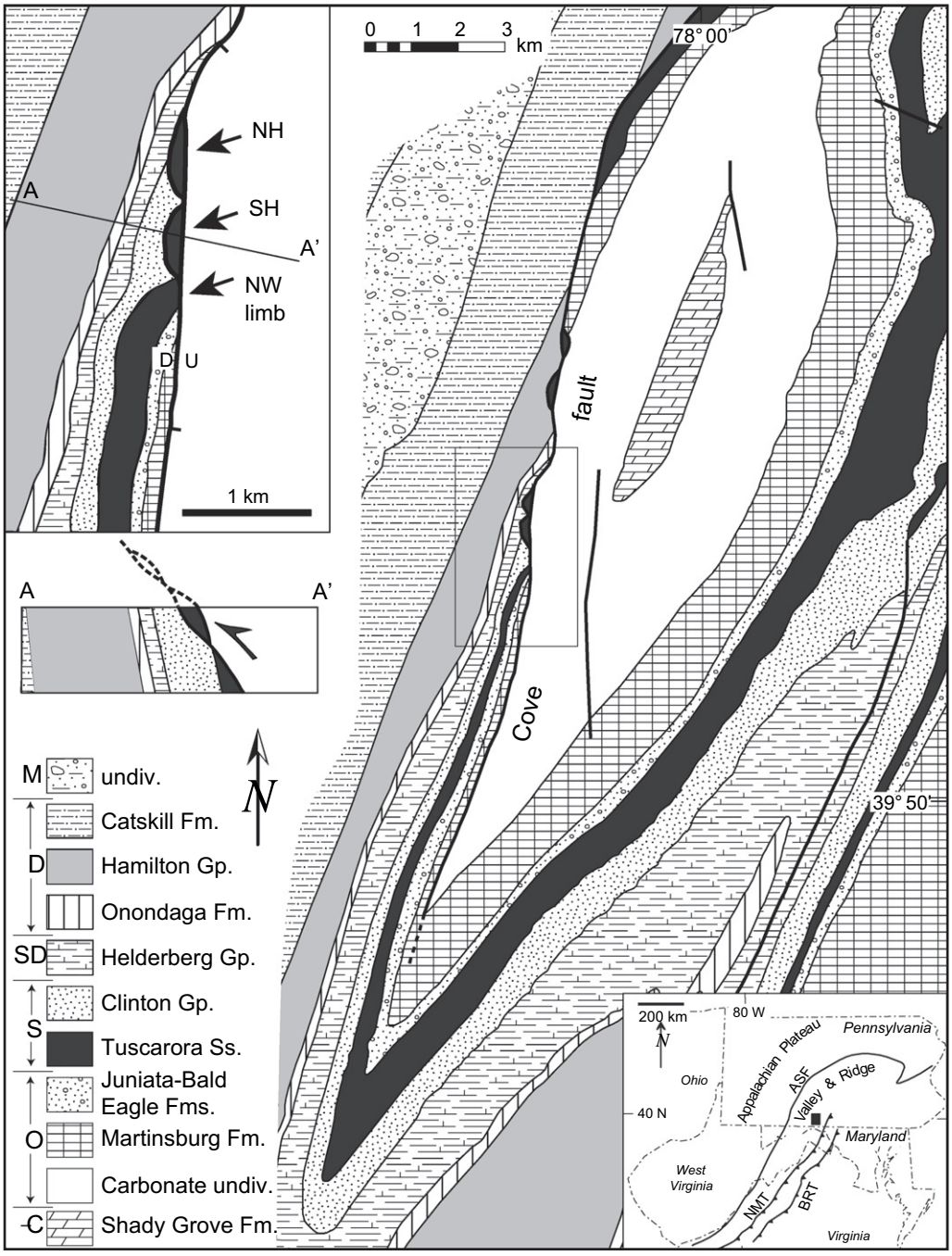

Fig. 1. Generalized geology of the Big Cove anticline. Detailed geology and cross section of boxed area in middle of map are shown in the upper left inset. Sampling localities are indicated in inset map with heavy arrows. NH – northern horse; SH – southern horse; NW limb – northwest limb. Inset map at lower right shows location of Big Cove anticline area (black box) relative to major structural features in central Appalachians. ASF – Appalachian structural front; NMT – North Mountain thrust; BRT – Blue Ridge thrust. Geology modified from Geologic Map of Pennsylvania (1960) and Nickelsen (unpublished data, 2003).

3. Methods

3.1. Microstructural characterization

Grain-scale deformation was characterized using transmitted and cathodoluminescence (CL) microscopy on oriented thin sections from 37 samples collected from the three sample sites. Sampling at the outcrop scale was done at variable distances from the contacts in the two horses and from the northern termination of the northwest limb. Thin section locations within hand samples were chosen to be as representative as possible of the structures visible in the sample. Microstructural abundances in six thin sections from each of the three sample sites (Fig. 1), chosen to be representative of those locations were quantified by point-counting. In each section, 200 counts were done along a grid with a node spacing of at

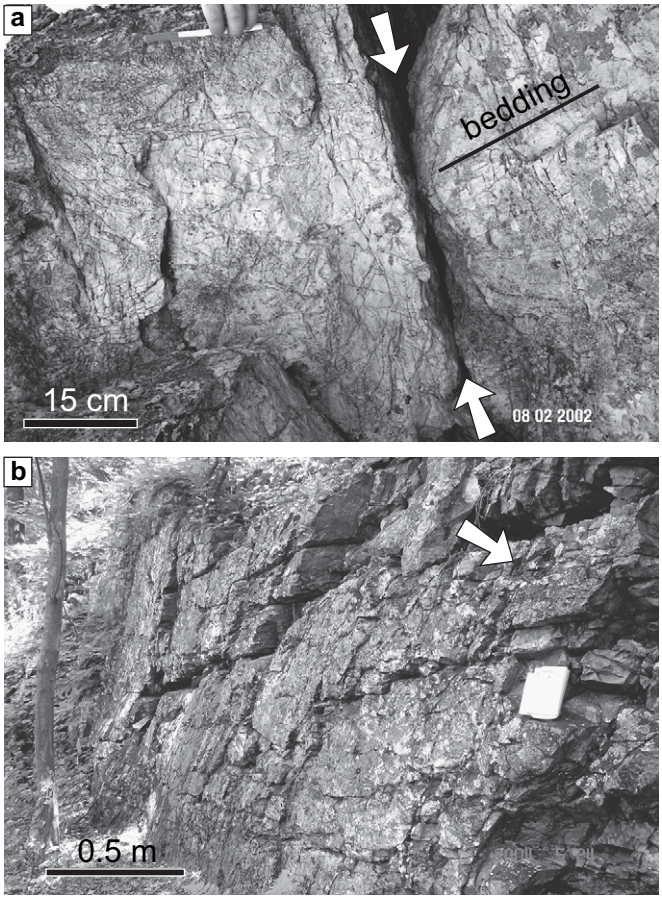

Fig. 2. Nature of mesoscopic faults in study area. (a) Steep, south-dipping minor fault (indicated by arrows) in southern horse. Bedding is presumed to dip gently to the left (NW) as seen by faint laminations. Although the fault is striated, the amount of displacement cannot be determined due to lack of recognizable stratigraphic markers. Note abundance of small fractures adjacent to fault. (b) Steep, northwest-dipping fault surface in northern horse. Many of the irregularities on the fault surface, such as the one indicated by the arrow, are due to dissolution.

least 4–5 grain diameters. At each grid node, the grain under the cross hairs was surveyed for microstructures, which were recorded as being present or absent. From these data, the abundances of both individual microstructures and of microstructures grouped by deformation mechanism were calculated separately for each sample site by averaging the six sections from that site. To provide a background comparison, microstructural abundances of 15 samples of the Tuscarora Sandstone from gently-dipping, southeast anticlinal limbs in the central Appalachian foreland (including the Big Cove anticline), deformed under similar P/T conditions and devoid of any mesoscopic structural complications (e.g., faults) were included (Onasch and Dunne, 1993). Microstructures are assumed to reflect deformation of the Tuscarora Sandstone. Evidence that they formed in situ and are not inherited from the sediment source rocks is shown by preferred microstructural orientations (Onasch, 1984), cross-cutting relations between microstructures, and microstructures (e.g., deformation lamellae) that extend from detrital grains into pore-filling cement (Onasch and Dunne, 1993).

3.2. Fluid inclusion microthermometry

Fluid inclusion microthermometry was used to estimate the physical and chemical conditions during the growth of quartz cement in nine samples. Doubly polished plates (100–200 μm-thick) were prepared by the methods of Goldstein and Reynolds (1994). Before inclusions were measured, they were mapped using CL so that the data could be separated on the basis of the CL color of the host quartz. For each quartz CL color, the homogenization temperature (T_h), last ice melting temperature (T_m), and eutectic temperature (T_e) of inclusions were measured to estimate the temperature, salinity, and salt composition, respectively, of the fluid at the time of crystal growth. Wherever possible, both T_h and T_m were measured for the same inclusion; however, the small size precluded the measurement of T_m in some inclusions. Both T_h and T_m measurements were reproducible to 0.1 °C. All samples were cooled to −120 °C to check for the presence of CO_2 and CH_4 and crushed in kerosene to detect the presence of organic gases (e.g., CH_4).

3.3. Oxygen isotope geochemistry

To constrain the fluid source, the $\delta^{18}O$ of quartz from two microveins and two cataclasite bands was measured. For comparison, two samples of the wallrock adjacent to the microveins and two adjacent to the cataclasite bands were also measured. Cataclasite band and microvein samples were prepared by hand-picking grains from a 100 μm-thick plate that was fractured in situ after being attached to sticky tape. Wallrock samples were prepared by homogenizing a minimum of 20 randomly-picked detrital grains from a distance of at least 2 mm from the microvein or cataclasite band. All data are reported in ‰ VSMOW (corrected to NBS-28) and have a precision of ±0.2‰ (1σ). Duplicates were run for each sample.

3.4. Fourier transform infrared spectrometry (FTIR)

The amount and distribution of intracrystalline water were investigated using FTIR. Depending on the nature of the target, spectral data were collected from single spots or along line scans using a Perkin Elmer Spectrum GX Fourier Transform Infrared Spectrometer (FTIR) with microscope accessory. In most cases, a 100 μm × 100 μm aperture was used so that spectra could be collected from detrital grain interiors, avoiding grain boundaries that might have adsorbed water. Samples consisted of 100–200 μm-thick, doubly polished plates. This thickness was sufficient to ensure a high count rate, but not so great as to encounter three-dimensional effects of vertically-stacked grains. The grain size of quartz in cataclasite and microveins is in the order of 5–50 μm making it unavoidable that multiple grains would have been included in a single aperture window. Smaller apertures of 30 μm or 50 μm were used with these features to minimize the number of grains sampled. Spectra were recorded in the range 2400–4000 cm^{-1} and reduced by removing the background. In most cases, a stable spectrum was obtained after 64 scans per spot.

Of the various water wavelength peaks on the IR spectra, the 3400 nm peak has proven to be the most useful (Kronenberg and Wolf, 1990; Nakashima et al., 1995) and was used here. Water concentration in H/10^6 Si was calculated as follows:

$$\text{Water concentration} = (\varepsilon \times A_{\text{cor}})/t \times 10^4 \quad (1)$$

where, ε is the absorption coefficient, A_{cor} is the area under the absorption curve determined through integration of the 3400 nm peak after removal of background, and t is the thickness of the sample in microns determined using a digital micrometer (Nakashima et al., 1995). A value of 1.05 was used for the absorption coefficient based upon the calibration of broad adsorption bands in synthetic quartz (Aines et al., 1984; Kronenberg, 1994). Recent calibration of a Black Hills quartzite sample using Karl Fisher titration indicates this value may systematically underestimate the water content (Stipp et al., 2006). Hence, the values reported here represent minimum water contents.

A total of 123 FTIR analyses were performed on 11 samples, primarily in the southern and northern horses. Targets in the samples included detrital grains with well developed crystal-plastic microstructures, quartz in microveins, and quartz cement in cataclasite. For comparison, grains lacking any visible microstructures (i.e., undeformed), mostly from the northwest limb were included as background.

4. Grain-scale deformation

The wide range of microstructures observed indicates that the Tuscarora Sandstone in the Cove fault zone deformed by several deformation mechanisms, operating sequentially and/or simultaneously. Brittle microstructures predominate in the northwest limb and the two horses with up to 72% of all grains in some thin sections displaying one or more brittle microstructures (Fig. 3). Brittle microstructures include, in order of decreasing abundance, transgranular and intragranular fluid inclusion planes (FIP), quartz microveins (Fig. 4b), cataclasite (Fig. 4a), and patchy extinction. Fluid inclusion planes are healed Mode I fractures (Tuttle, 1949; Groshong, 1988). They are ubiquitous in all sample localities and reach densities as high as 100 mm^{-1} in the two horses. Although orientations were not systematically measured, no preferred orientation was observed in thin sections. Microveins are also Mode I fractures (Onasch, 1990; Blenkinsop, 2000), but have dilated to widths of 10–500 μm and are filled with quartz cement that is in optical continuity with wallrock grains. They generally lack any FIP indicating that they are younger. The cataclasite consists of a mosaic of fine-grained quartz with or without identifiable detrital grains or grain fragments. It occurs both as irregular areas (Figs. 4a and b, 6a–d) and in variably oriented tabular zones 10–1000 μm wide (Fig. 4c and d). In the northern horse, distributed and tabular zones of cataclasite comprise up to 30% of the rock. The tabular zones tend to lack obvious wallrock fragments common in the distributed cataclasite and consist primarily of a mosaic of fine-grained (5–10 μm diameter) quartz (Fig. 4d). Although shear can be demonstrated across some cataclasite bands, most show only dilation. Cross-cutting generations of cataclasite (Fig. 4a) indicate multiple episodes of formation. Patchy extinction consists of sharply bounded domains within detrital grains with slightly different (1–5°) extinction positions. The boundary between extinction domains is thought to be an array of healed microcracks across which a small amount of rotation has occurred (J. Tullis, personal communication, 2006). Compared to regional background samples, rocks in the Cove fault zone display a much greater abundance of brittle microstructures (Fig. 3a).

Crystal-plastic microstructures are second-most abundant in the fault zone (Fig. 3). Up to 25% of grains in the northern horse contain sweeping undulose extinction, deformation lamellae, and/or deformation bands (Fig. 4e). Although not included in the point-counting, a few highly deformed grains also show evidence of grain-boundary migration recrystallization, such as highly serrated grain boundaries or boundaries marked with small polygonal grains. Crystal-plastic microstructures are less abundant in the Cove fault zone than in regional background samples, especially for deformation lamellae and deformation bands (Fig. 3a). However, in contrast to background samples, a spatial relationship between crystal-plastic and other microstructures was observed in the Cove fault zone: grains adjacent to FIP swarms, microveins, and dissolution surfaces often contain more crystal-plastic microstructures, such as deformation lamellae, deformation bands, and large-angle undulose extinction, than those away from these features. To illustrate this relationship, the amount of lattice distortion in grains with sweeping undulose extinction was estimated using the angular difference between extinction positions. This approach assumes that the variation in extinction angle within a grain is due to plastic deformation of the lattice (Blenkinsop, 2000). It is apparent from Fig. 5 that the greatest lattice distortions occur in the vicinity of dissolution surfaces. It was also noted that grains with pronounced undulose extinction, as well as deformation lamellae and bands, can be distinguished in plane-polarized light by a brownish tint resulting from clouds of inclusions <1 μm in diameter (Figs. 4f and 5b).

Pressure solution microstructures are least abundant in the Cove fault zone (Fig. 3) with less than 5% of grains in each sample site showing sutured or interpenetrated grain–grain contacts, or transgranular stylolites (Fig. 4b and f). These abundances are comparable to regional background values (Fig. 3a). Despite the low abundance of pressure solution microstructures determined from point-counting, evidence for dissolution is very prominent in outcrop where goethite-filled stylolites and surfaces with cavities with up to several centimeters of relief are prominently displayed on or near mesoscopic faults (Fig. 2b). Also prevalent in these zones are irregular, goethite-filled vugs, up to several centimeters in diameter, containing quartz grains and quartz arenite rock fragments with highly irregular, scalloped boundaries (Fig. 6e and f).

The abundance of different microstructures at the three sample sites varies systematically from south to north. All microstructures, except microveins, are most abundant in the

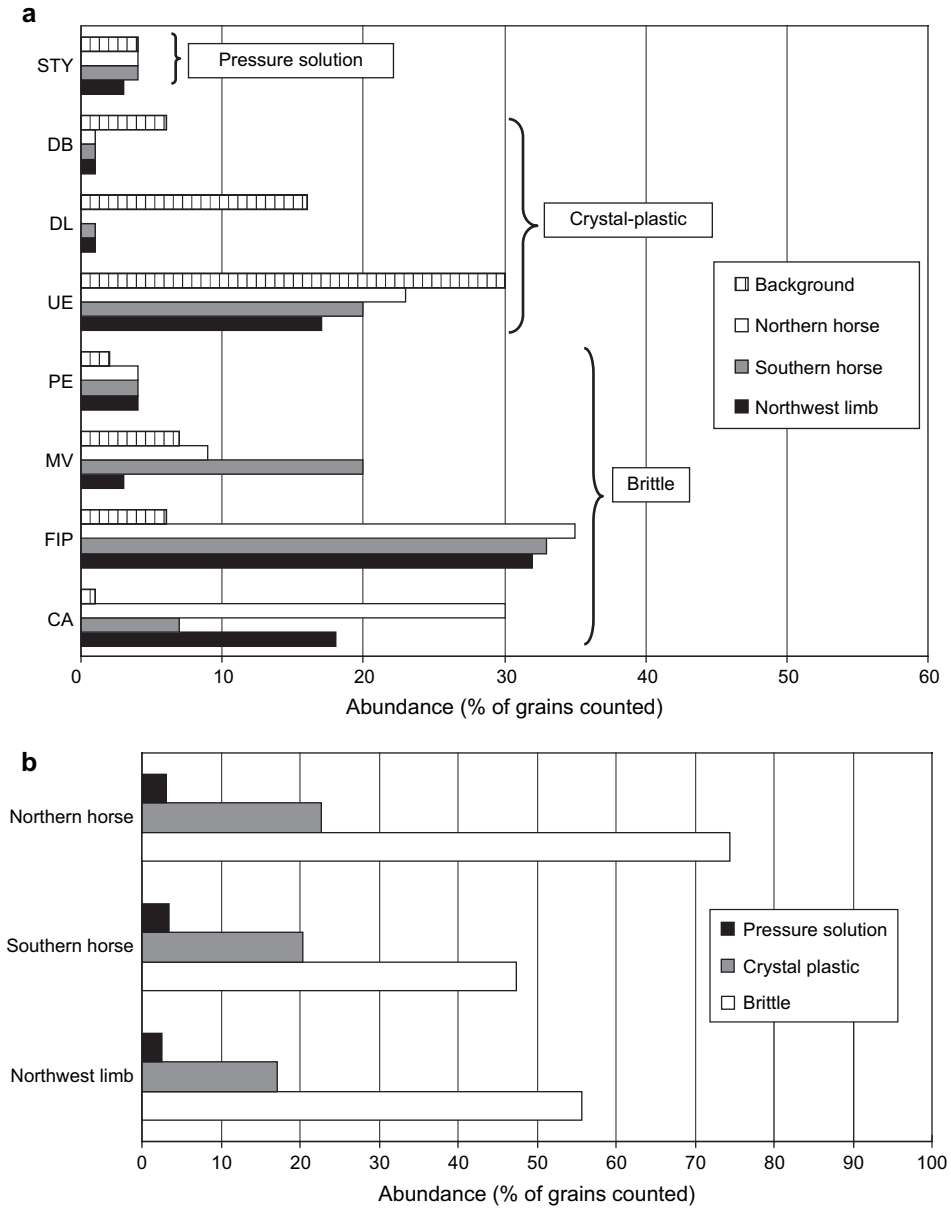

Fig. 3. Microstructural abundances. (a) Abundance of individual microstructures in the three sample sites with a comparison to background samples. Abundance is the percent of the total grains counted ($n = 200$) that contain that microstructure. STY – transgranular stylolites and sutured grain contacts; DB – deformation bands; DL – deformation lamellae; UE – undulose extinction; PE – patchy extinction; MV – microveins; FIP – intragranular and transgranular fluid inclusion planes; CA – cataclasite. (b) Abundance of microstructures grouped by their parent deformation mechanism. Groupings are: pressure solution – STY; crystal-plastic – UE + DL + DB; brittle – PE + MV + FIP + CA.

northern horse and least abundant in the northwest limb (Fig. 3a). This trend is more apparent when microstructures are grouped by their parent deformation mechanism (Fig. 3b). The south to north trend of increasing microstructure abundance corresponds to the progressive obliteration of bedding as seen in outcrop and to an increase in the number of surfaces presumed to be faults (Fig. 2).

As demonstrated by cross-cutting relations between microstructures, the general progression through time was from brittle to crystal-plastic to pressure solution-dominated deformation. The earliest deformation in the fault zone created zones of distributed cataclasite, followed by formation of the tabular zones of cataclasite, which cut the distributed cataclasite (Fig. 4a). Next were FIP, and then microveins, which cut all earlier microstructures (Figs. 4b and 6b). Overlapping in time with formation of FIP and microveins are crystal-plastic microstructures such as deformation lamellae and deformation bands. Crystal-plastic deformation continued beyond the formation of some microveins as the quartz fill has undulose extinction. Pressure solution structures, such as goethite-filled stylolites, are generally the youngest features as they cut all other microstructures (Figs. 4b and f, 6e and f) except the goethite-filled fractures and vugs, which appear to be coeval. Some crystal-plastic deformation was coeval with pressure

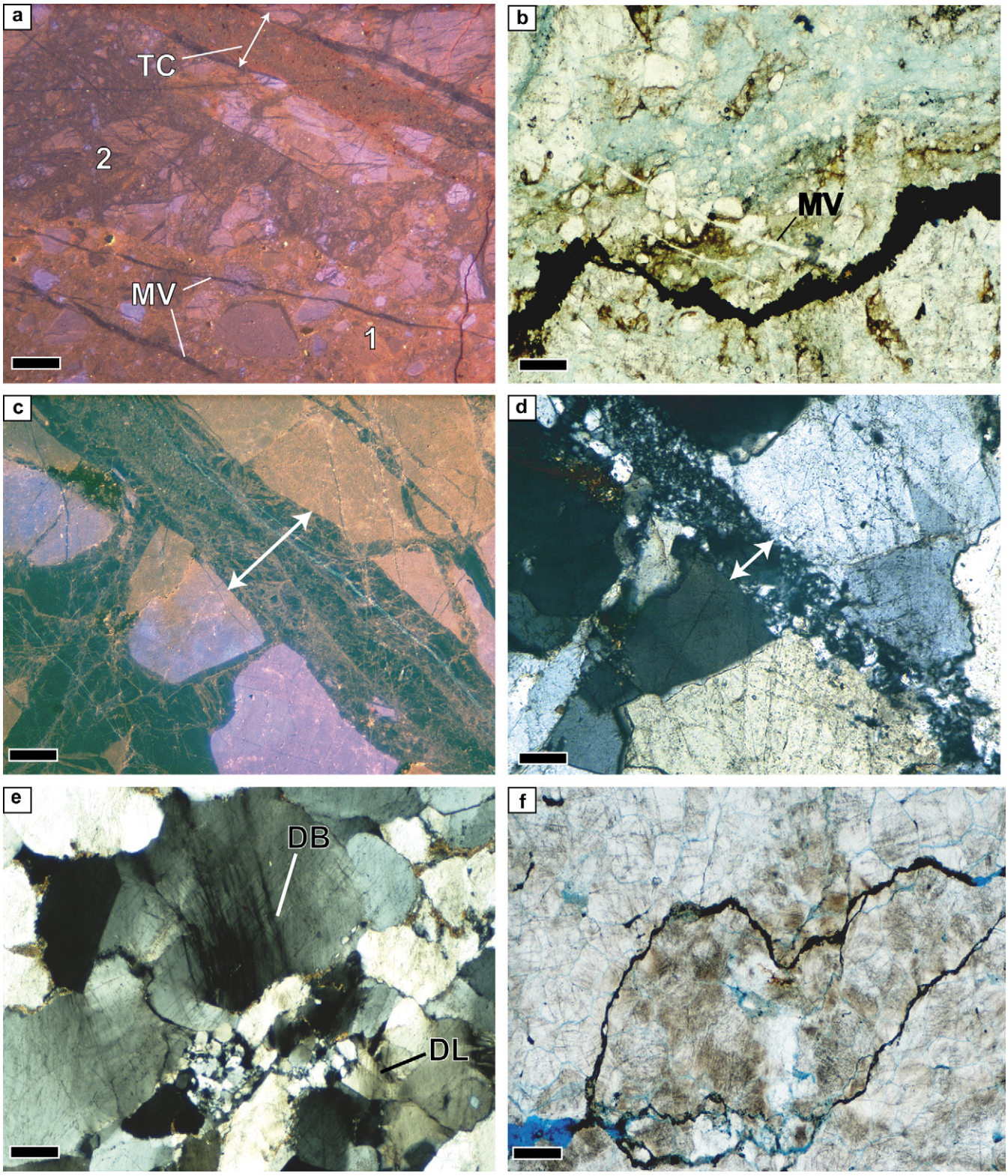

Fig. 4. Photomicrographs of grain-scale structures. (a) CL view of two generations (1 = older; 2 = younger) of distributed cataclasite cut by tabular zone of cataclasite (TC) and microvein (MV). (b) Plane-polarized light view of distributed cataclasite and microveins (MV) cut by goethite-filled dissolution surfaces. Blue tint is dye in epoxy. (c) CL view of tabular cataclasite zone. Note luminescence of zone is similar to cement in adjacent microveins. (d) Crossed-polarized light view of same area as (c). Note that zone in polarized light is significantly narrower than in CL, indicating significant dilation and filling by quartz growing syntaxially on detrital wallrock grains. (e) Deformation bands (DB) and deformation lamellae (DL) in detrital quartz grains. (f) Aggregate of detrital grains surrounded by goethite-filled dissolution surfaces. Brownish tint of the grains is a result of abundant submicroscopic inclusions. Grains with this tint have more crystal-plastic microstructures than those outside the aggregate and very high intragranular water contents as measured by FTIR. Scale bar in all photomicrographs is 100 μm.

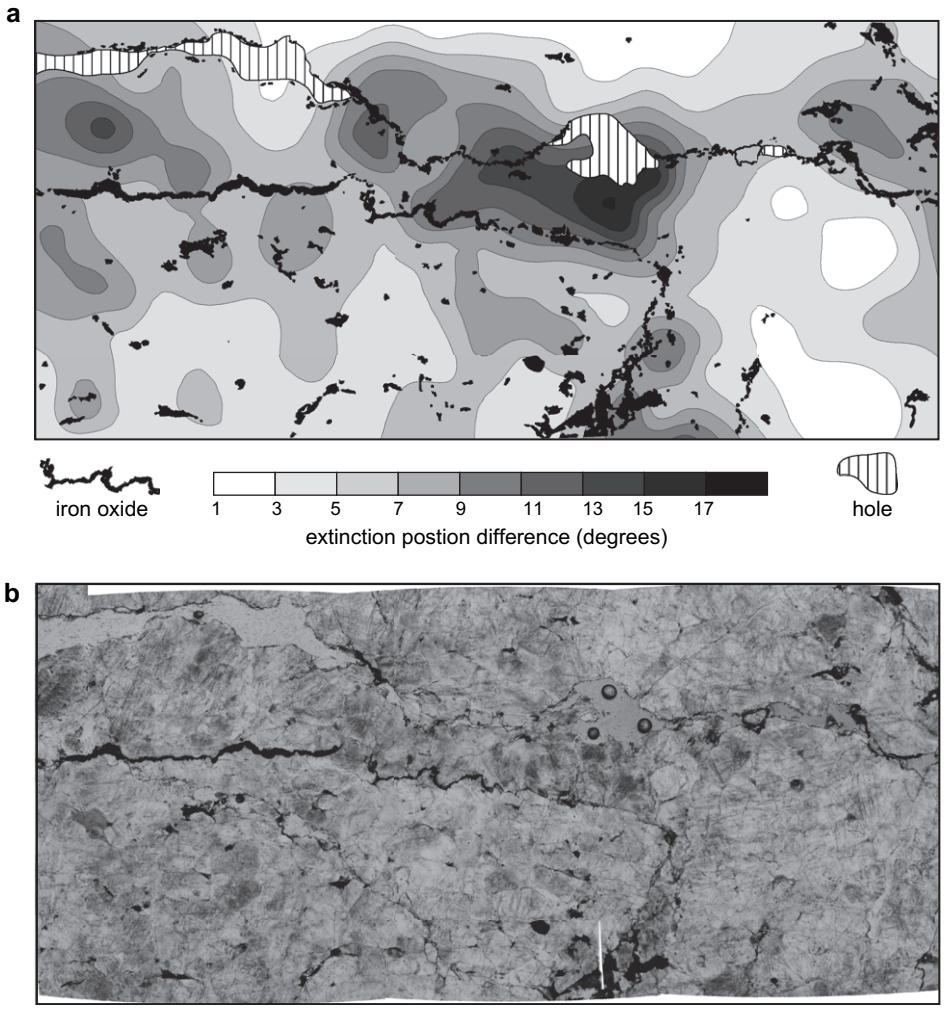

Fig. 5. Spatial relationship between quartz grain lattice distortion and fluid pathways. (a) Contoured map of lattice distortion, as measured by the angular difference between extinction positions in grains ($n = 150$) with undulose extinction, overlain by iron oxide accumulations. Iron oxide lies along dissolution surfaces (stylolites) and in pores. Holes in sample were mostly filled with iron oxide that was plucked during sample preparation. Note the strong correlation between grains with large lattice distortions and location of dissolution surfaces, especially in the area between two sub-horizontal surfaces in center of map. (b) Plane-polarized photomicrograph mosaic of area in (a). Note that grains with large lattice distortions tend to be clouded with inclusions, as in brown-tinted grains in Fig. 4f. Width of map and mosaic is 8 mm.

solution as shown by the localization of crystal-plastic microstructures adjacent to well developed stylolites (Figs. 4f and 5).

5. Fluids

Based on differences in CL, fluid inclusion data, oxygen isotope analyses, and mineralogy, three different fluids were present at different times during the evolution of the Cove fault zone (Table 1). Initial discrimination of different fluids was made using the CL color of the quartz precipitated by that fluid. Once separated by CL color, fluid inclusion microthermometry, stable isotope geochemistry, and FTIR were used to more thoroughly characterize the fluids.

5.1. Fluid I

Quartz precipitated by Fluid I has a concentrically zoned, dark reddish-brown luminescence (Table 1) and is found as cement in the distributed and tabular cataclasite, and in the oldest microveins (Fig. 6a). The zoning consists of ~10 μm wide zones of alternating CL intensity in which narrower zones, <5 μm wide, are found.

Fluid inclusions in microveins consist of two-phase aqueous inclusions, 2–10 μm in diameter. T_h values range from 147.4 °C to 241.7 °C with a mode of 190 °C (Fig. 7a). T_m values range from −11.0 °C to −23.0 °C with a mode of −20 °C (Fig. 7b) corresponding to 22.7 wt.% NaCl equivalent. The T_e of approximately −50 °C indicates that the fluid is a $CaCl_2$-rich brine. In a few samples, crushing experiments yielded expanding vapor bubbles that dissolved in kerosene indicating the presence of an organic gas, most likely CH_4. Due to the narrow width of the microveins and presence of detrital grain fragments in cataclasite, quantities of quartz sufficient to determine the oxygen isotopic composition of the quartz associated with Fluid I could not be collected.

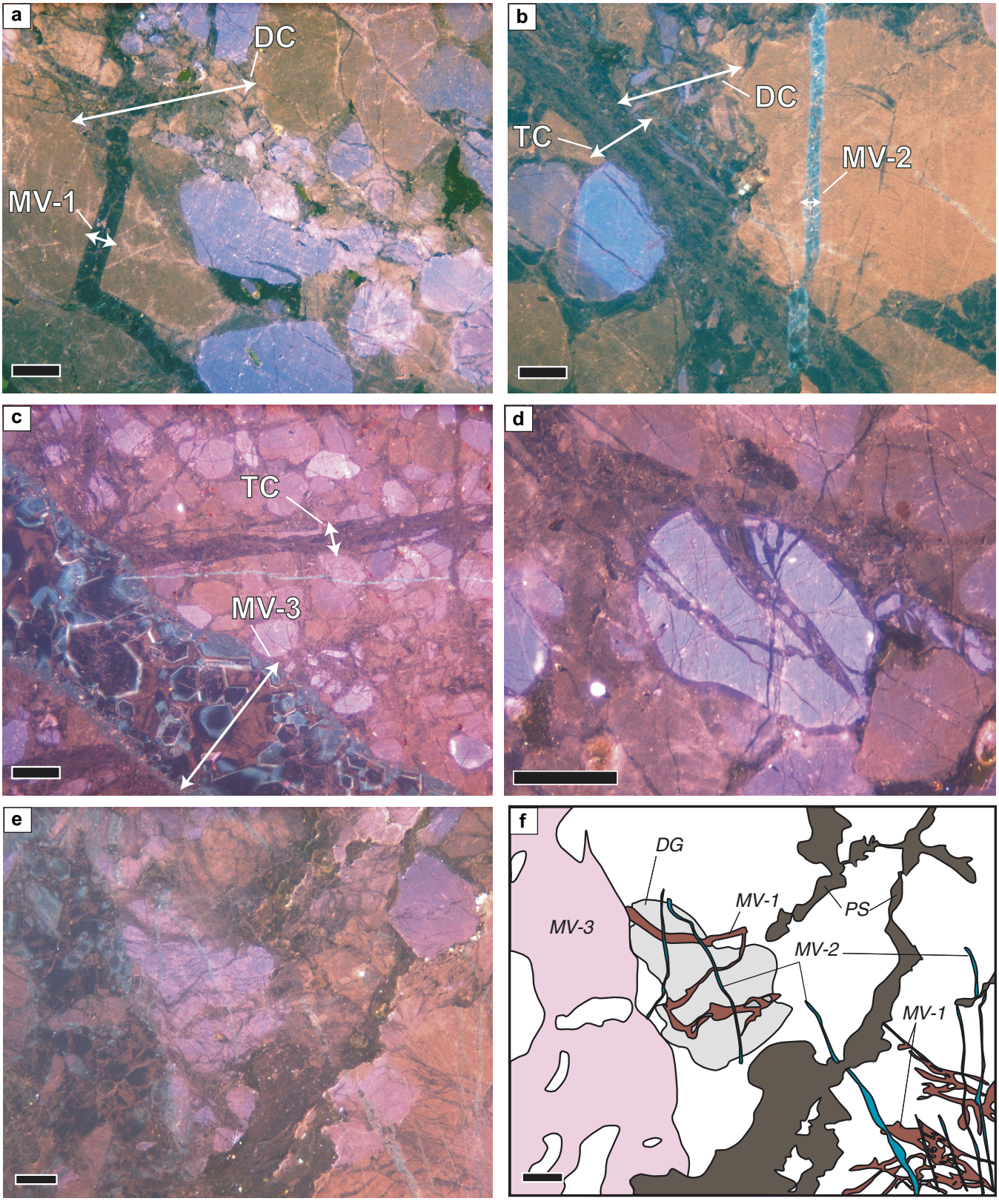

Fig. 6. Photomicrographs of grain-scale and fluid-related features. (a) CL view of oldest generation microvein (MV-1) cutting detrital grains and zone of distributed cataclasis (DC). (b) CL view of second generation microvein (MV-2) cutting detrital grain and tabular zone of cataclasis (TC), which cuts area of distributed cataclasis (DC), (c) CL view of youngest generation microvein (MV-3) cutting tabular zone of cataclasis (TC). Note pronounced zoning of quartz from reddish-brown to bluish-green in microvein. (d) CL view of detrital grain with fracture filled with cataclasite from surrounding area, all of which is cut by younger, narrow microvein. (e) CL view of sample showing relative age relations between microstructures. (f) Schematic diagram of (e); DG – plastically deformed detrital grain; MV-1, 2, 3 – three generations of microveins (1 = oldest), each with different luminescence; PS – irregular zone of dissolution filled with goethite. Relative age sequence, from oldest to youngest, is DG, MV-1, MV-2, MV-3, and PS. Scale bar in all photomicrographs is 100 μm.

Table 1
Characteristics of fluids and minerals precipitated by fluids in Cove fault zone

	Mineral precipitated	CL color	Fluid inclusion type	T_h (°C)	T_m (°C)	Wt.% NaCl equiv.	T_e (°C)	Dominant salt
Fluid I	Quartz	Reddish-brown	2-phase, aqueous, +/−CH_4	190[a]	−20[a]	22.7	Approximately −50	$CaCl_2$
Fluid II	Quartz	Bluish-green	2-phase aqueous, +/−CH_4	200[b]	−18[a]	21.2	Approximately −50	$CaCl_2$
Fluid III	Goethite	n/a	n/a	n/a	n/a	n/a	n/a	n/a

Quartz precipitated from Fluid I was sampled from cataclasite cement and microveins, whereas that for Fluid II was from microveins.
[a] Modal temperature.
[b] Median temperature.

5.2. Fluid II

Quartz precipitated from Fluid II has a striking concentrically zoned, bright bluish-green luminescence (Table 1) and is found in microveins that cut cataclasite and older microveins cemented with reddish-brown luminescing quartz (Fig. 6b). Like the reddish-brown luminescing quartz from Fluid I, the bluish-green luminescence is zoned on two scales: ~10 μm and <5 μm.

Fluid inclusions in these microveins consist of two-phase aqueous inclusions, 2–8 μm in diameter. T_h values range from 154.5 °C to 250.6 °C. Although the modal T_h is slightly

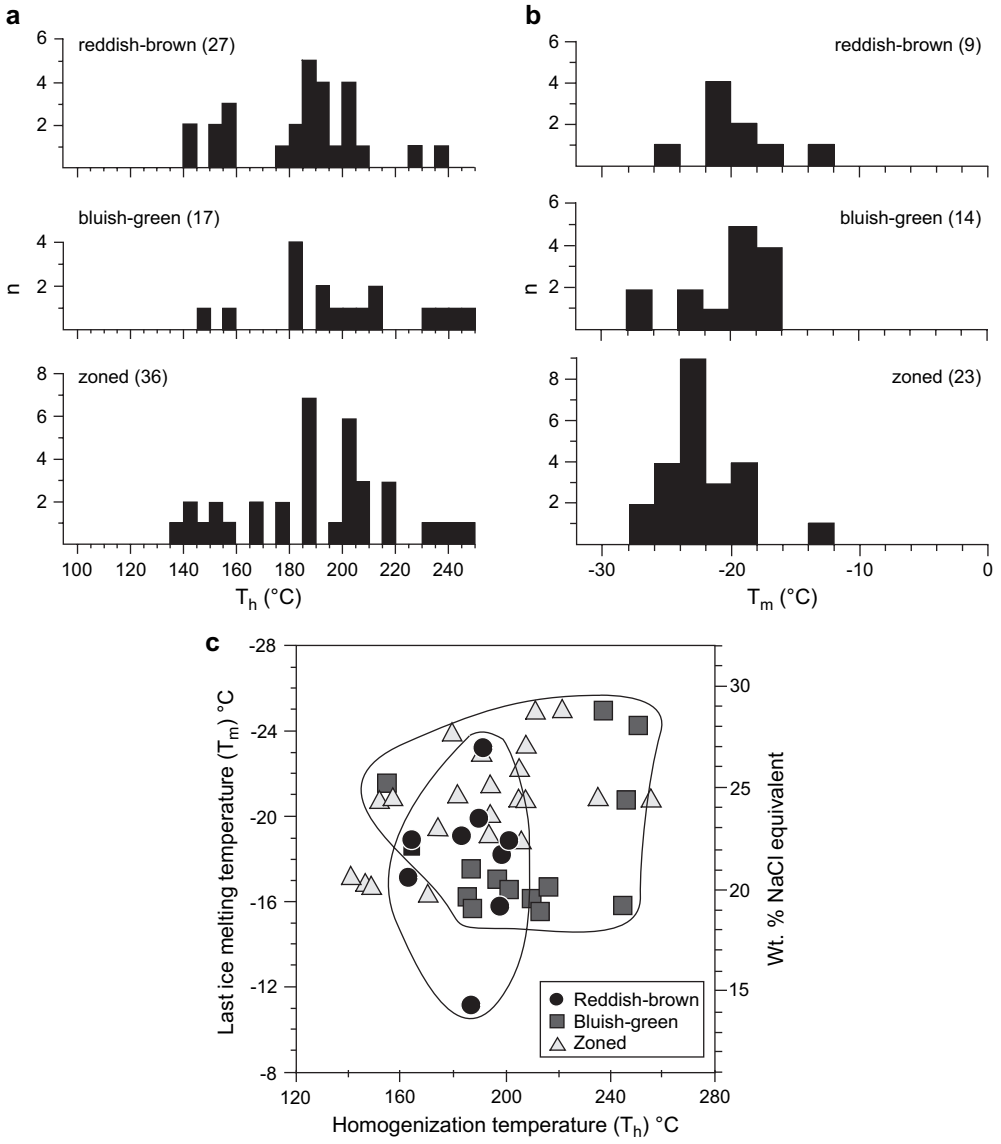

Fig. 7. Fluid inclusion microthermometry data. (a) Histograms of homogenization temperatures (T_h) for inclusions differentiated by luminescence color of host quartz. Number in parentheses is the number of inclusions measured. Zoned luminescence data are from microveins which contain alternations of both reddish-brown and bluish-green luminescing quartz. (b) Histograms of last ice melting temperatures (T_m) for three luminescence colors. (c) Plot of T_h versus T_m for 48 inclusions from which both T_h and T_m were measured. T_m is also expressed as weight % NaCl equivalent. Inclusions from reddish-brown and bluish-green quartz grouped to highlight population differences.

lower than that for Fluid I inclusions (Fig. 7a), the data are more positively skewed suggesting a higher T_h. This difference is more apparent on a plot of T_h versus T_m where the center of the grouping of inclusions from bluish-green quartz is at a higher temperature than that for the reddish-brown quartz (Fig. 7c). For the purposes of discussion, the median T_h of 200 °C will be used to represent this population of inclusions. T_m values range from −15.4 °C to −24.8 °C with a mode of −18 °C (Fig. 7b) corresponding to an NaCl equivalent salinity of 21.2 wt.%. The T_e value of approximately −50 °C indicates the fluid is also a $CaCl_2$-rich brine. Crushing experiments indicate that a few inclusions contain an organic gas, probably CH_4.

The $\delta^{18}O$ of bluish-green luminescing quartz in microveins is similar to that in tabular cataclasite zones, with means of 26.0‰ and 25.1‰, respectively (Table 2). Wallrock compositions are significantly lighter, averaging 15.8‰ (Table 2). The oxygen isotopic composition of the fluid in equilibrium with quartz from Fluid II can be estimated using the fractionation factor from Clayton et al. (1972) and assuming equilibrium fractionation. The median T_h of 200 °C from the microvein fluid inclusion data yields a fluid composition of 14.3‰. Because the T_h is a minimum estimate for the temperature of crystal growth, this is a minimum estimate of the fluid composition.

5.3. Fluid III

Fluid III is associated with the precipitation of goethite (Table 1) in fractures, along stylolites (Fig. 4b and f), and in vugs (Fig. 6e and f). As quartz was not precipitated from this fluid, no luminescence, fluid inclusion, or stable isotope data were obtained.

6. Distribution of water in quartz

All targets show considerable variation between grains within samples; however, some trends are apparent. The lowest water concentrations were found in quartz filling the microveins, which has a mean water content of 5104 H/10^{-6} Si (Table 3). The highest concentrations were found in detrital grains with crystal-plastic microstructures, which have a mean of 16,979 H/10^{-6} Si (Table 3; Fig. 8). In many cases, these high concentrations were found in brownish grains localized near FIP swarms or dissolution surfaces (Figs. 4f and 5). The water content in quartz from the tabular zones of cataclasite shows the largest variation and has a mean of 10,691 H/10^{-6} Si (Table 3; Fig. 8). By comparison, grains lacking visible microstructures have a water content averaging 9387 H/10^{-6} Si (Table 3). Line scans across microveins and tabular zones of cataclasite show pronounced drops in water content relative to wallrock grains (Fig. 9).

The water concentrations measured in samples from the Cove fault zone exceed by at least two orders of magnitude the maximum amount of water that can be dissolved in the quartz lattice under equilibrium conditions. McConnell et al. (1995) predicted that water, as $(4H)_{Si}$ defects, would reach a maximum concentration of 200 H/10^{-6} Si at 600 °C with little effect of pressure (Gerretsen et al., 1987). Brazil quartz is considered to be very "dry" and typically has <50 H/10^{-6} Si incorporated as point defects (Kronenberg et al., 1986), whereas milky quartz is considered to be "wet" with a water content of ~2000 H/10^{-6} Si, incorporated mostly as sub-optical freezable fluid inclusions (Aines and Rossman, 1985). Previous studies of deformed rocks have found water in concentrations higher than even these "wet" quartz values, but considerably lower than those in the Cove fault zone. Kronenberg and Wolf (1990) reported water contents of 3800–4100 H/10^{-6} Si in experimentally deformed Heavitree Quartzites, whereas Kronenberg et al. (1990) found values between 3000 and 8000 H/10^{-6} Si in mylonite samples. Nakashima et al. (1995) found a systematic increase in water in quartz from granites from 600 to 5000 H/10^{-6} Si that correlates to an increase in deformation.

Water can exist in quartz as Si-OH (silanol) in the crystal structure, non-freezable liquid water in nanometer-sized water clusters, and freezable liquid water in fluid inclusions (Kronenberg, 1994). Previous FTIR studies of water in quartz (e.g., Kronenberg and Wolf, 1990; Kronenberg et al, 1990) do not consider optical-scale fluid inclusions in the interpretation of their results; therefore, the water in quartz of the Cove fault zone measured by FTIR is assumed to exist as silanol defects and nanometer-sized water clusters.

Table 2
Oxygen isotope analyses of quartz

Sample	Type	$\delta^{18}O$ (VSMOW)
CF-21	CB	26.0
CF-21 dup.	CB	26.0
CF-23	CB	23.9
CF-23 dup.	CB	24.4
CF-7	VN	26.3
CF-7	VN	25.5
CF-7 dup.	VN	26.2
CF-5	WR	14.3
CF-7	WR	15.9
CF-7 dup.	WR	15.9
CF-21	WR	16.7
CF-21 dup.	WR	16.6
CF-23	WR	15.3

CB, cataclasite band; VN, vein; WR, wallrock. (CB & VN are related to Fluid II).

Table 3
Intragranular water concentrations measured by FTIR

Target	Water concentration (H/10^6 Si)		
	Min	Max	Mean
Undeformed detrital grains $n=4$; $m=54$	1672	19,425	9387
Deformed detrital grains (with brown tint) $n=2$; $m=22$	9107	25,747	16,979
Quartz in cataclastic bands $n=3$; $m=30$	302	20,448	10,691
Quartz in microveins $n=2$; $m=17$	419	11,556	5104

n, Number of samples analyzed; m, number of spots within the samples analyzed.

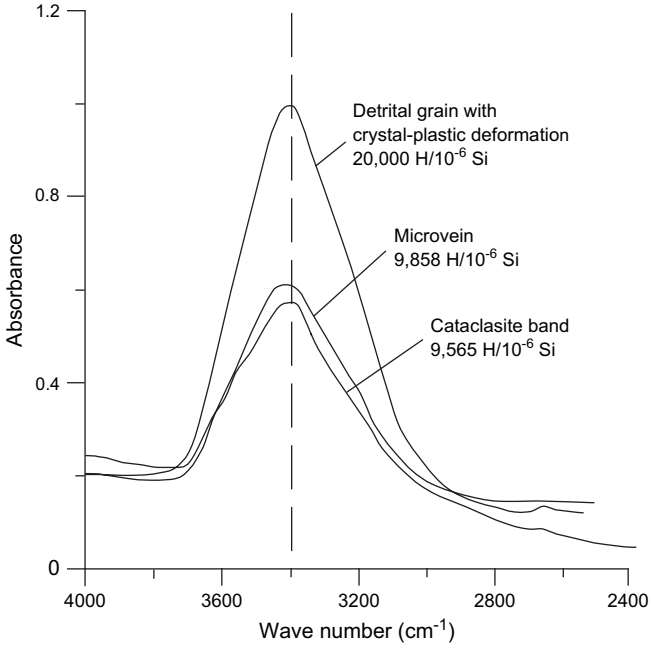

Fig. 8. Sample IR spectra of three different types of quartz: crystal-plastically deformed detrital grain, microvein, and tabular cataclasite zone. Spectra were smoothed with a three-point running average. Water concentration, in H/10^6 Si, is proportional to area under 3400 cm^{-1} peak and includes water in Si-OH defects and in nanometer-sized water clusters.

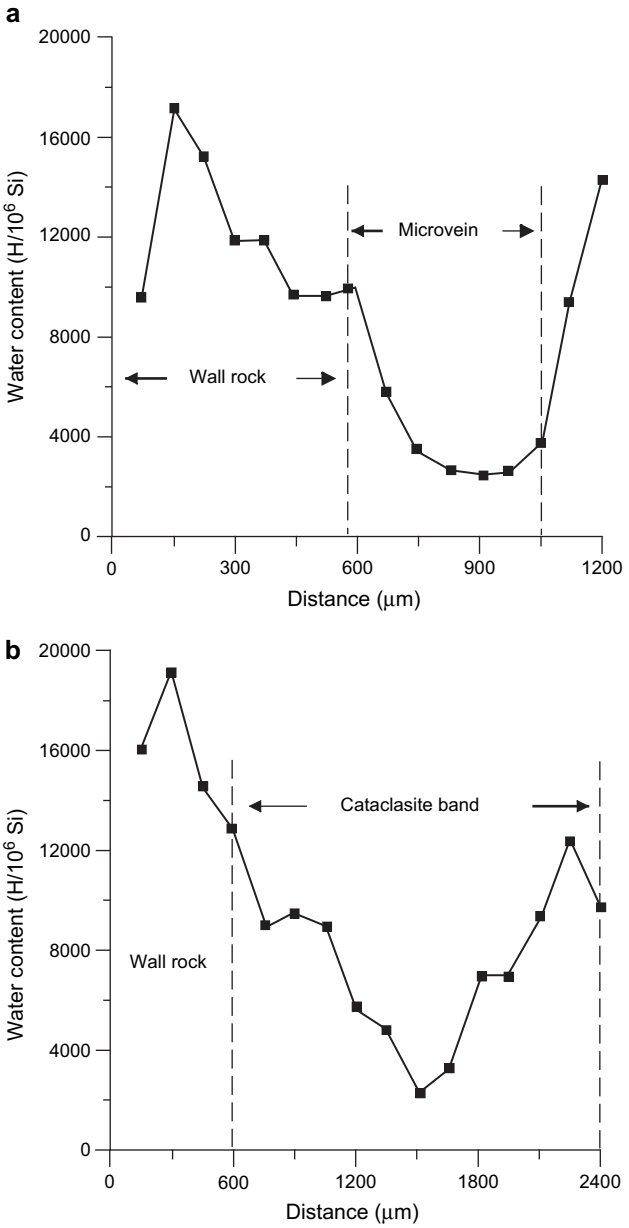

Fig. 9. Variation in water concentration in quartz grains determined from IR line scans across (a) microvein, and (b) cataclasite band. Width of box at each data point is equal to width of aperture (30 × 30 μm). Note similar water concentration within microvein and cataclasite band.

7. Discussion

Microstructures and textures clearly show that fluids were present in the Cove fault zone throughout much of its deformation history. Evidence for fluids includes quartz cement in cataclasite and microveins, fluid inclusions in healed microfractures (FIP), dissolution microstructures (stylolites, sutured and interpenetrated grains), and intragranular water concentrations in quartz grains that are greatly in excess of equilibrium solubility values. The central question to be addressed here is what role, if any, did these fluids play in controlling the selection of grain-scale deformation mechanisms? To answer this question, we must look at the temporal and spatial relationships between the microstructures and the fluid history.

7.1. Deformation-fluid history

The timing relationships between grain-scale deformation and the three fluids are shown in Fig. 10 and can be largely surmised from cross-cutting relations shown in Fig. 6e and f. The earliest deformation is the distributed and localized cataclasis that produced cataclasite cemented with reddish-brown luminescing quartz precipitated from a $CaCl_2$ brine (Fluid I). Fluid pressures must have been great enough to allow dilation and cementation of the cataclasite. The injection of cataclasite into dilated fractures (Fig. 6d) is further evidence of high fluid pressures. Overprinting relations show that localized cataclasis persisted after distributed cataclasis (Fig. 4a), which may reflect a change in the bulk behavior of the rock. At the start of deformation, weaknesses localized along the boundaries of incompletely cemented detrital grains failed in response to a shear stress leading to distributed cataclasis. Cementation of this cataclasite by quartz from Fluid I strengthened the rock resulting in a shift from distributed to localized brittle failure along variably oriented tabular zones and discrete shear surfaces. The nature of brittle deformation changed again, possibly in response to a change in the rate of displacement on the Cove fault, when widely distributed Mode I fracturing (FIP and microveins) replaced cataclasis as the dominant mode of deformation. Quartz precipitated from Fluid I continued to cement these microfractures at a rate sufficient to prevent loss of cohesion and cataclasis. The low intragranular water content

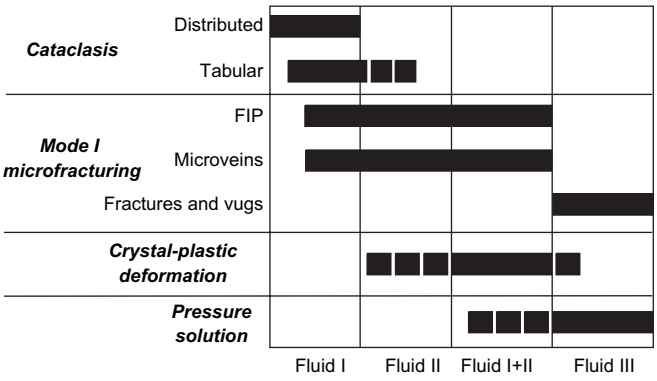

Fig. 10. Temporal relationships between grain-scale deformation history and different fluids in Cove fault zone.

of the quartz filling microveins (Table 3) is a consequence of orderly growth that would minimize the number of water-related defects being incorporated into the lattice. The low water content of the cataclasite bands argues against the fine-grained quartz fill originating by comminution of wallrock grains, which typically have high water contents (Table 3). Rather, these bands are thought to be dilational structures that fill with quartz precipitated rapidly from a silica supersaturated solution (Farver and Onasch, 2003; Onasch et al., 2006). The temperature during dilational microfracturing can be estimated from the fluid inclusion data. Correcting for a pressure corresponding to hydrostatic conditions at a depth of 7 km (Epstein et al., 1977; Harris et al., 1978; Onasch and Dunne, 1993; Evans and Battles, 1999), the modal T_h of 190 °C for a fluid with 22.7 wt.% NaCl equivalent salinity yields a trapping temperature of 225 °C.

The luminescence color of the quartz cement also yields information on the physical and/or chemical conditions during deformation. Luminescence color is a function of the number and type of crystal defects and/or impurity ions in the lattice (Marshall, 1988; Muller et al., 2003; Gotze et al., 2005; Boggs and Krinsley, 2006). Reddish-brown luminescence in quartz, such as that precipitated by Fluid I, is attributed to Al impurities in the lattice (van den Kerkhof et al., 2001; Muller et al., 2003). The conspicuous concentric zoning in the cataclasite cement and microvein fill could then be a result of systematic variations in the amount of Al in Fluid I. It is also possible for concentric zoning to form without changing the bulk composition of the fluid through geochemical self-organization (Sibley et al., 1976; Pearce and Kolisnik, 1990; D'Lemos et al., 1997). In this process, the rate of incorporation of an element (i.e., Al) into the growing crystal exceeds the rate at which that element can diffuse through the fluid to the growth surface resulting in an episodic depletion of that element in the fluid adjacent to the growth surface until diffusion reestablishes equilibrium. This episodic variation in element concentration in the growing crystal results in oscillations in the intensity of the luminescence (Rusk et al., 2006). Of the two possible causes for the zoning, we favor geochemical self-organization because it does not require numerous, abrupt changes in the bulk chemistry of Fluid I.

As microfracturing, possibly under high fluid pressures, continued to dominate the grain-scale deformation, the composition of the fluid in this part of the Cove fault zone changed to that of Fluid II as indicated by the change in the luminescence color of quartz cements from reddish-brown to bluish-green (Fig. 6b). Bluish-green luminescence in quartz is unusual in the central Appalachians and has not been observed by the authors in the Tuscarora Sandstone or other units outside the Cove fault zone. Bluish-green luminescence has been attributed to Ti impurities in the lattice (van den Kerkhof et al., 2001; Ruffini et al., 2002), and has been described from Ti-rich magmatic systems (van den Kerkhof et al., 2004). While the change in luminescence color of quartz cements from Fluids I and II marks a change in bulk fluid composition, the origin of the concentric zoning in the bluish-green quartz is believed to be the same as that in the reddish-brown quartz from Fluid I: geochemical self-organization. Judging from the fluid inclusion data, the salinity may have also decreased somewhat from that of Fluid I (Table 1; Fig. 7b and c). The temperature during this part of the deformation, estimated from the Fluid II median T_h corrected for hydrostatic conditions at a depth of 7 km, was 235 °C, slightly higher than that for the earlier deformation. Because the temperature did not change significantly, the growing importance of crystal-plastic deformation is attributed to an increase in the intragranular water content or fugacity to the point where ambient stress levels were sufficient to induce dislocation nucleation and motion. The preferential development of crystal-plastic microstructures near fluid conduits like FIP, microveins, and dissolution surfaces (Figs. 4f and 5) supports this interpretation. It also indicates that microfracturing, pressure solution, and crystal-plastic deformation must have been operating simultaneously as all types of microstructures overprint each other.

The youngest microveins are filled with alternations of concentrically zoned reddish-brown and bluish-green luminescing quartz (Fig. 6c) indicating that both Fluids I and II were present (Fig. 10). Whereas alternations in the intensity of luminescence are thought to result from geochemical self-organization, alternations between two distinctly different colors (i.e., reddish-brown and bluish-green), indicate pulses of different fluids with different trace element chemistries. Consistent with this interpretation are the fluid inclusion data from these microveins which show homogenization temperatures and salinities that overlap those of quartz from Fluids I and II (Fig. 7). Pressure solution, as shown by grain-to-grain suturing and transgranular stylolites, began to contribute more to the deformation as crystal-plastic microstructures continued to form. Temperatures for this portion of the deformation were similar to those for deformation in the presence of Fluids I and II, 225–235 °C.

The youngest part of the deformation marks a major change in rock behavior and fluid chemistry. Whereas Fluids I and II were silica-rich, Fluid III was iron-rich (Table 1). Coeval with Fluid III were large transgranular stylolites that cross-cut all other microstructures (Fig. 4a and f), pitting of fault surfaces (Fig. 2b), and grains and rock fragments with deeply embayed

margins within goethite-lined vugs indicate that a significant amount of quartz dissolution occurred at this time (Fig. 10). Overlapping in time with the stylolites are transgranular fractures and vugs, both filled with goethite. The goethite along the dissolution surfaces was not derived from dissolution of wallrock grains, which lack iron oxides; rather, it was precipitated from Fluid III along the stylolite surfaces. This requires that they dilated subsequent to their formation by compaction in response to a change in stress field geometry or increased fluid pressure. Therefore, these solution structures differ from stylolites in the traditional sense because the goethite is not a passive accumulation of insoluble material, but a precipitate from a later event.

The simultaneous precipitation of iron oxide and dissolution of quartz presents somewhat of a paradox, as the two processes would appear to require different fluid chemistries. At a given pressure and temperature, quartz solubility is favored by a high pH whereas the transport of iron oxide in solution requires a low pH (Walther, 2005). A possible solution to this paradox may lie in redox reactions whereby the conversion of dissolved ferrous iron to the ferric state increases the solubility of quartz and also causes iron oxide to precipitate (Morris and Fletcher, 1987). Applying this model, ferrous iron in Fluid III reacted with quartz to form a microlayer of hydrous ferrous silicate. Under oxidizing conditions, this layer broke down to form a goethite precursor and released silica into solution. Repeated episodes of this process resulted in the replacement of quartz by goethite; however, it is not known what mechanism might allow for repeated changes in redox conditions.

7.2. Origin of the fluids

The source of a fluid can be inferred from its salinity and isotopic composition. Fluid I and II salinities of 22.7 and 21.2 wt.% NaCl equivalent (Table 1), respectively, suggest a basinal brine. The fluids in equilibrium with the quartz in veins and cataclasite bands have $\delta^{18}O$ values of 14.3‰ and 13.4‰, respectively, (Table 2), which is consistent with a basinal brine ($\delta^{18}O$ of up to 30‰) that has partially equilibrated with the host rocks (Hoefs, 1997), a metamorphic fluid (5–25‰) (Taylor, 1974), or a mixture of the two. Regionally in the central Appalachian foreland, the fluids responsible for vein mineralization are believed to have been derived from the hinterland during metamorphism and mixed with brines and hydrocarbons during their migration to the foreland (Evans and Battles, 1999). This migration was stratified by the differing permeabilities of existing rock units. The aquifer that includes the Tuscarora Sandstone was dominated by high salinity, CH_4-saturated brines (Evans and Battles, 1999)

Fluids in the Cove fault zone differ from those described by Evans and Battles (1999) elsewhere in the central Appalachians. Although temperatures and salinities overlap (Fig. 11), those in the Cove fault zone have less methane, are heavier isotopically (Fig. 11), and precipitated quartz with an unusual bluish-green luminescence. Although some methane was found during crushing experiments of fluid inclusions, those inclusions were in the minority and, unlike the results of Evans and Battles (1999), no single-phase, CH_4-rich inclusions were found.

The distinctive isotopic composition of the fluids in the Cove fault zone, relative to those elsewhere in the Appalachian foreland (Fig. 11), can be explained by an isotopically heavier source and/or less fluid-rock interaction during flow. Whereas the fluids described by Evans and Battles (1999) are thought to have traveled from the metamorphic hinterland through stratigraphically-controlled aquifers, those in the Cove fault zone may have come up along the fault from a more local source. Because the Cove fault zone acted as a major fluid conduit with channelized flow, fluids would have undergone less exchange with isotopically lighter wallrocks than in the regional fracture networks sampled by Evans and Battles (1999) where the flow was more dispersed. The channelized flow would also have provided less opportunity for mixing with hydrocarbons from units in the hanging and footwalls, which would explain the relative lack of methane in the Cove fault zone.

7.3. Did fluids affect selection of grain-scale deformation mechanisms?

We have shown that aqueous fluids were present throughout most, if not all, of the deformation in the Cove fault zone and that the nature of grain-scale deformation changed with time as different fluids permeated the fault zone. Here, we address the possibility that these fluids were responsible for the changing nature of the grain-scale deformation.

Deformation of quartz-rich rocks in a fault zone at depths of 7 km and 200–250 °C is expected to be dominantly brittle, especially if strain rates are high (Sibson, 1977; Lloyd and Knipe, 1992). In the Cove fault zone, the early deformational history was brittle leading to the formation of distributed cataclasite. Once this cataclasite was cemented, brittle deformation continued, but by displacement along and across discrete fracture surfaces or within narrow zones.

Although brittle microstructures are most abundant in the Cove fault zone, crystal-plastic deformation was locally important. The occurrence of extensive undulose extinction, deformation lamellae, deformation bands, and some evidence for grain-boundary migration recrystallization, at temperatures below 250 °C, can be explained by the presence of water. The FTIR analysis showed that many grains with crystal-plastic microstructures have exceptionally high water concentrations that are nearly double the concentration in grains lacking these microstructures (Table 3). Once in the lattice, water lowers the flow stress in two ways: (1) nano-scale water clusters promote hydrolytic weakening (Kronenberg, 1994; Post et al., 1996); and (2) micron-scale inclusions provide nucleation sites for dislocations (FitzGerald et al., 1991). Because it facilitates the formation and motion of dislocations, water would allow crystal-plastic deformation to occur at temperatures lower than would otherwise be required for a given differential stress. How water enters the lattice is still not well understood (Kronenberg, 1994; Post and Tullis, 1998). At temperatures below 300 °C, diffusion rates are too slow for water to penetrate to the center of grains several hundred μm in diameter

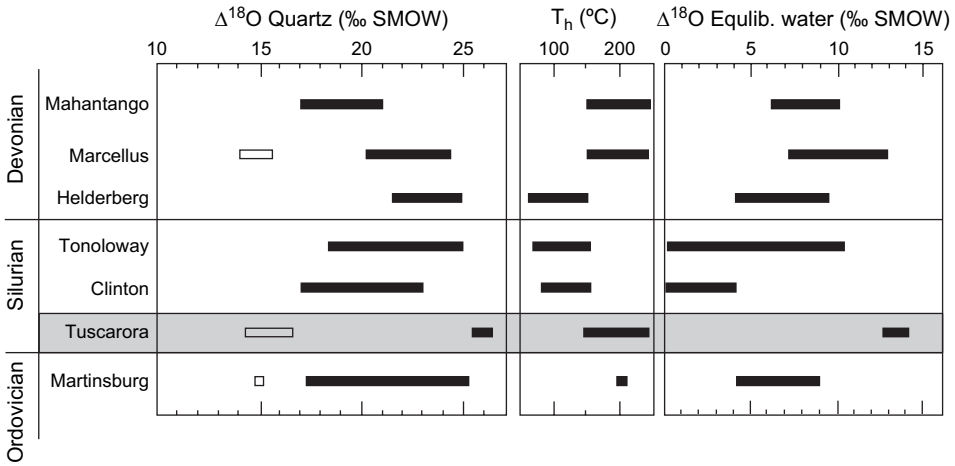

Fig. 11. Comparison of fluid-related parameters between those measured in Tuscarora Sandstone from the Cove fault zone in this study (shaded box) and those measured by Evans and Battles (1999; Fig. 9) in the Virginia and West Virginia portion of the Appalachian foreland. All data come from veins except for open bars in quartz oxygen isotope plot, which are from wallrock.

(Post and Tullis, 1998). Kronenberg (1994) and Kronenberg et al. (1990) suggest that dilatant microfracturing delivers water to grain interiors where only a small amount of diffusion would be necessary for water to reach any part of the grain. The abundant healed microfractures (FIP) in samples from the Cove fault zone and their proximity to the grains with crystal-plastic microstructures are consistent with that model. Once crystal-plastic deformation begins, it can facilitate further hydrolytic weakening by allowing additional water diffusion through dislocation cores (Heggie and Jones, 1986; Heggie, 1992). The effect of crystal-plastic deformation on preexisting healed microfractures is not clear. Some grains with deformation lamellae and bands or extensive sweeping undulose extinction still contain abundant FIP. Others, however, are devoid of them, but contain abundant submicron inclusions that give the grains the brownish tint (Figs. 4f and 5b) suggesting that if FIP were originally present, they have been removed by the crystal-plastic deformation.

The change from quartz precipitation to widespread dissolution in the later stages of deformation also appears to have been controlled by the fluids, only this time it was a change in fluid chemistry that promoted the change in deformational style. With the introduction of iron in the fluid, redox reactions led to the precipitation of goethite as well as the enhanced solubility of quartz. Large amplitude stylolites and extensive pitting of grain surfaces were the result. In comparison to dissolution, brittle deformation appears to be unimportant at this time, which may have been brought about by a decrease in the rate of displacement in the fault zone. The decrease in crystal-plastic deformation indicates that strain was more easily accommodated by dissolution than by crystal-plastic deformation.

7.4. Implications for the rheology of fault zones

Rocks in the Cove fault zone experienced more brittle deformation and less crystal-plastic deformation than background samples from gently-dipping fold limbs (Fig. 3b). This is to be expected in a fault zone where strain rates are higher than in rocks undergoing regional deformation (Sibson et al., 1979; Lloyd and Knipe, 1992). The Cove fault also shows evidence for an evolution in grain-scale deformational processes. We have shown that through time, the behavior of quartz arenite in the fault zone changed from brittle to ductile, in response to variations in the amount and chemistry of fluids.

The evolution from cataclasis to ductile deformation is common in fault zones (Stewart et al., 2000; Imber et al., 2001; Holdsworth, 2004; Jefferies et al., 2006). Microfracturing associated with early cataclasis facilitates access of water to the fault zone, which promotes diffusive mass transport and mineral reactions leading to the formation of weak layer silicate phases. Except for the formation of layer silicates, which would not be expected in a quartz arenite deformed at low temperatures, the history of the Cove fault zone is consistent with this model. It is also possible that the shift from brittle to ductile deformation in the Cove fault zone reflects the timing of fault displacement relative to the evolution of the Cove Mountain anticline. Because the fault developed relatively late in the regional deformational history (R. Nickelsen, personal communication, 2003), it is likely that the Cove Mountain anticline continued to tighten during and after faulting. The shift from brittle to ductile deformation within the fault zone may reflect the change from faulting to ductile attenuation of the northwest limb of the Cove Mountain anticline.

8. Conclusions

Aqueous fluids, through both mechanical and chemical effects, controlled the nature of grain-scale deformation, and hence the rheology, of the Cove fault zone. Early brittle deformation led to distributed cataclasis. Cementation of the cataclasite by quartz precipitated from aqueous fluids changed the behavior of the rock, which led to dilation and/or shear

displacement along discrete surfaces and in narrow zones. Where fluid pathways such as pervasive microfracturing or dissolution surfaces were present, intragranular water concentrations reached sufficiently high levels to allow crystal-plastic deformation to become locally important, despite temperatures below 250 °C. Finally, a change in fluid chemistry in the latter stages of deformation within the fault zone resulted in widespread dissolution of quartz and precipitation of goethite.

Acknowledgements

The authors are indebted to Richard P. Nickelsen who introduced them to this area and generously shared his unpublished data. Access to key portions of the study area was provided by Mr. Ralph Glenn. Financial support was provided by NSF grant EAR 0087607 to Onasch and Farver, and by the Richard D. Hoare Research Fund at Bowling Green State University to O'Kane. Discussions with Mark Evans helped clarify interpretations of the fluid inclusion data and comments from William Dunne, Anne-Marie Boullier, and Jan Tullis greatly improved the manuscript.

References

Aines, R.D., Kirby, S.H., Rossman, G.R., 1984. Hydrogen speciation in synthetic quartz. Physics and Chemistry of Minerals 11, 204–212.

Aines, R.D., Rossman, G.R., 1985. The high temperature behavior of trace hydrous components in silicate minerals. American Mineralogist 70, 1169–1179.

Ashby, M.F., 1972. A first report on deformation mechanism maps. Acta Metallica 20, 887–897.

Atkinson, B.K., 1984. Subcritical crack growth in geological materials. Journal of Geophysical Research 89, 4077–4114.

Blenkinsop, T., 2000. Deformation Microstructures and Mechanisms in Minerals and Rocks. Kluwer Academic Publishers, Dordrecht.

Boggs, S., Krinsley, D., 2006. Application of Cathodoluminescence Imaging to the Study of Sedimentary Rocks. Cambridge Press, Cambridge.

Boullier, A.-M., Robert, F., 1992. Paleoseismic events recorded in Archean gold–quartz vein networks, Val d'Or, Abitibi, Quebec, Canada. Journal of Structural Geology 14, 161–179.

Caine, J.S., Evans, J.P., Forster, C.B., 1996. Fault zone architecture and permeability structure. Geology 24, 1025–1028.

Carter, N.L., Kronenberg, A.K., Ross, J.V., Wiltschko, D.V., 1990. Control of fluids on deformation of rocks. In: Knipe, R.J., Rutter, E.H. (Eds.), Deformation Mechanisms, Rheology and Tectonics. Geological Society, London, Special Publications, vol. 54, pp. 1–14.

Clayton, R.N., Mayeda, T.K., O'Neil, J.R., 1972. Oxygen isotope exchange between quartz and water. Journal of Geophysical Research 77, 3057–3067.

Cook, J., Dunne, W.M., Onasch, C.M., 2006. Development of a dilatant damage zone along a thrust relay in a low-porosity quartz arenite. Journal of Structural Geology 28, 776–792.

Cotter, E., 1983. Shelf, paralic, and fluvial environments and eustatic sea-level fluctuations in the origin of the Tuscarora formation (Lower Silurian) of central Pennsylvania. Journal of Sedimentary Petrology 53, 25–49.

Cox, S.F., 1995. Faulting processes at high fluid pressures: an example of fault-valve behavior from the Wattle Gully Fault, Victoria, Australia. Journal of Geophysical Research 100, 841–859.

Cox, S.F., Braun, J., Knackstedt, M.A., 2001. Principles of structural control on permeability and fluid flow in hydrothermal systems. In: Richards, J.P., Tosdal, R.M. (Eds.), Structural Controls on Ore Genesis. Reviews in Economic Geology 14, 1–24.

D'Lemos, R.S., Kearsley, A.T., Pembroke, J.W., Watt, G.R., Wright, P., 1997. Complex quartz growth histories in granite revealed by scanning cathodoluminescence techniques. Geological Magazine 134, 549–552.

Den Brok, S.W.J., Spiers, C.J., 1991. Experimental evidence for water weakening of quartzite by microcracking plus solution–precipitation creep. Journal of the Geological Society of London 148, 541–548.

Epstein, A.G., Epstein, J.B., Harris, L.D., 1977. Conodont color alteration: an index to organic metamorphism. U.S. Geological Survey Professional Paper, pp. 1044–9612.

Evans, J.P., Forster, C.B., Goddard, J.V., 1997. Permeability of fault-related rocks and implications for hydraulic structure of fault zones. Journal of Structural Geology 19, 1393–1404.

Evans, M.A., 1989. The structural geology and evolution of foreland thrust systems, northern Virginia. Geological Society of America Bulletin 101, 339–354.

Evans, M.A., Battles, D.A., 1999. Fluid inclusion and stable isotope analyses of veins from the central Appalachian Valley and Ridge province: implications for regional synorogenic hydrologic structure and fluid migration. Geological Society of America Bulletin 111, 1841–1860.

Farver, J.R., Onasch, C.M., 2003. Nature and origin of cataclastic bands in well cemented quartz arenite. EOS Transactions, AGU 84 (46). T42D-08.

FitzGerald, J.D., Boland, J.N., McLaren, A.C., Ord, A., Hobbs, B.E., 1991. Microstructures in water-weakened single crystals of quartz. Journal of Geophysical Research 96, 2139–2155.

Geologic Map of Pennsylvania, 1960. Topographic and Geologic Survey of Pennsylvania.

Gotze, J., Plotze, M., Toralf, T., 2005. Structure and luminescence characteristics of quartz from pegmatites. American Mineralogist 90, 13–21.

Goldstein, R.H., Reynolds, T.J., 1994. Systematics of fluid inclusions in diagenetic minerals. In: SEPM Short Course 31.

Gerretsen, J., Paterson, M.S., McLaren, A.C., 1987. The uptake and solubility of water in quartz at elevated pressure and temperature. Tectonophysics 16, 334–342.

Griggs, D.T., Blacic, J.B., 1965. Quartz: anomalous weakness of synthetic crystals. Science 147, 292–295.

Groshong Jr R.H., 1988. Low-temperature deformation mechanisms and their interpretations. Geological Society of America Bulletin, vol. 100. pp. 1329–1360.

Harris, A.G., Epstein, J.B., Harris, L.D., 1978. Oil and gas data from Paleozoic rocks in the Appalachian basin: maps for assessing hydrocarbon potential and thermal maturity (conodont color alteration isograds and overburden isopachs). U.S. Geological Survey Professional Paper 0160–0753.

Hatcher Jr R.D., Thomas, W.A., Geiser, P.A., Snoke, A.W., Mosher, S., Wiltschko, D.V., 1989. Alleghanian orogen. In: Hatcher Jr R.D., Thomas, W.A., Viele, G.W. (Eds.), The Appalachian–Ouachita Orogen in the United States. The Geology of North America F-2, 233–318.

Heald, M.T., Anderegg, R.C., 1960. Differential cementation in the Tuscarora Sandstone (Virginia-West Virginia). Journal of Sedimentary Research 30, 568–577.

Heggie, M.I., Jones, R., 1986. Models of hydrolytic weakening in quartz. Philosophical Magazine Letters A53, L65.

Heggie, M.I., 1992. Molecular diffusion of oxygen and water in amorphous silica: role of basal dislocations. Philosophical Magazine Letters A65, 155–158.

Hoefs, J., 1997. Stable Isotope Geochemistry. Springer, New York.

Hirth, G., Tullis, J., 1992. Dislocation creep regimes in quartz aggregates. Journal of Structural Geology 14, 145–159.

Holdsworth, R.E., 2004. Weak faults-rotten cores. Science 303, 181–182.

Houseknecht, D.W., 1988. Intergranular pressure solution in four quartzose sandstones. Journal of Sedimentary Petrology 58, 228–246.

Hubbert, M.K., Rubey, W., 1959. Role of fluid pressure in mechanics of overthrust faulting. In: Geological Society of America Bulletin, vol. 70. pp. 115–166.

Imber, J., Holdsworth, R.E., Butler, C.A., 2001. A reappraisal of the Sibson–Scholtz fault zone model: the nature of the frictional to viscous (''brittle–ductile'') transition along a long-lived, crustal-scale fault, Outer Hebrides, Scotland. Tectonics 20, 601–624.

Jefferies, S.P., Holdsworth, R.E., Wibberley, C.A.J., Shimamoto, T., Spiers, C.J., Niemeijer, A.R., Lloyd, G.E., 2006. The nature and importance of phyllonite development in crustal-scale fault cores: an example from the median tectonic line, Japan. Journal of Structural Geology 28, 220–235.

Knipe, R.J., 1989. Deformation mechanisms – recognition from natural tectonites. Journal of Structural Geology 1, 127–146.

Knipe, R.J., 1992. Faulting processes and fault seal. In: Larsen, R.M. (Ed.), Structural and Tectonic Modeling and its Applications to Petroleum Geology, Stavanger, NPF, pp. 325–342.

Kronenberg, A.K., 1994. Hydrogen speciation and chemical weakening of quartz. In: Heaney, P.J., Prewitt, C.T., Gibbs, G.V. (Eds.), Silica, Physical Behavior, Geochemistry and Materials Applications. Reviews in Mineralogy 29, 123–176. Mineralogical Society of America.

Kronenberg, A.K., Wolf, G.H., 1990. Fourier transform infrared spectroscopy determinations of intragranular water content in quartz-bearing rocks: implications for hydrolytic weakening in the laboratory and within the earth. Tectonophysics 172, 255–271.

Kronenberg, A.K., Kirby, S.H., Aines, R.D., Rossman, G.R., 1986. Solubility and diffusional uptake of hydrogen in quartz at high water pressure: implications for hydrolytic weakening. Journal of Geophysical Research 91, 12723–12744.

Kronenberg, A.K., Segall, P., Wolf, G.H., 1990. Hydrolytic weakening and penetrative deformation within a natural shear zone. In: Durham, W.B., Handin, J.W., Wang, H.F. (Eds.), Geophysical Monograph, vol. 56. American Geophysical Union, Washington, DC, pp. 21–36.

Laubach, S.E., 1997. A method to detect natural fracture strike in sandstones. American Association of Petroleum Geologists Bulletin 81, 604–623.

Laubach, S.E., Lander, R., Bonnell, L., Olson, J., Reed, R., 2004. Opening histories of fractures in sandstone. In: Cosgrove, J.W., Engelder, T. (Eds.), The initiation, propagation, and arrest of joints and other fractures. Geological Society, London, Special Publications, vol. 231, pp. 1–9.

Lespinasse, M., 1999. Are fluid inclusion planes useful in structural geology? Journal of Structural Geology 21, 1237–1243.

Lloyd, G.E., Knipe, R.J., 1992. Deformation mechanism accommodating faulting of quartzite under upper crustal conditions. Journal of Structural Geology 14, 127–143.

Logan, J.M., 1991. The influence of fault zones on crustal-scale fluid transport (abs). AAPG Bulletin 75, 623.

Marshall, D.J., 1988. Cathodoluminescence of Geological Materials. Unwin Hyman, Boston.

McCaig, A.M., 1989. Fluid flow through fault zones. Nature 340, 600.

McConnell, J.D.C., Lin, J.S., Heine, V., 1995. The solubility of [4H]Si defects in a quartz and their role in the formation of molecular water and related weakening on heating. Physics and Chemistry of Minerals 22, 357–366.

Morris, R.C., Fletcher, A.B., 1987. Increased solubility of quartz following ferrous–ferric iron reactions. Nature 330, 558–561.

Muller, A., Wiedenbeck, M., van den Kerkhof, A.M., Kronz, A., Simon, K., 2003. Trace elements in quartz – a combined electron microprobe, secondary ion mass spectrometry, laser-ablation ICP-MS, and cathodoluminescence study. European Journal of Mineralogy 15, 747–763.

Nakashima, S., Matayoshi, H., Yuko, T., Michibayashi, K., Masuda, T., Kuroki, N., Yamagishi, H., Ito, Y., Nakamura, A., 1995. Infrared microspectroscopy analysis of water distribution in deformed and metamorphosed rocks. Tectonophysics 245, 263–276.

Onasch, C.M., 1984. Petrofabric test of viscous buckling theory. Tectonophysics 106, 141–153.

Onasch, C.M., 1990. Role of microfractures in the deformation of a quartz arenites in the central Appalachian foreland. Journal of Structural Geology 12, 883–894.

Onasch, C.M., Dunne, W.M., 1993. Variation in quartz arenite deformation mechanisms between a roof sequence and duplexes. Journal of Structural Geology 5, 465–476.

Onasch, C.M., Farver, J.R., Dunne, W.M., 2006. Cataclasite bands in well cemented quartz arenite: a product of shear or rapid dilation? In: Geological Society of America, Abstracts with Programs, vol. 38, p. 310.

Paterson, M., 1989. The interaction of water with quartz and its influence in dislocation flow – an overview. In: Karato, Shun-ichiro (Ed.), Rheology of Solids and of the Earth. Oxford University Press, pp. 107–142.

Paterson, M.S., Luan, F.C., 1990. Quartzite rheology under geological conditions. Geological Society of London, Special Publications, vol. 54. pp. 299–307.

Pearce, T.H., Kolisnik, A.M., 1990. Observations of plagioclase zoning using interference imaging. Earth Science Reviews 29, 9–26.

Pollard, D.D., Aydin, A., 1988. Progress in understanding jointing over the past century. Geological Society of America Bulletin 100, 1181–1204.

Post, A.D., Tullis, J., 1998. The rate of water penetration in experimentally deformed quartzite: implications for hydrolytic weakening. Tectonophysics 295, 117–138.

Post, A.D., Tullis, J., Yund, R.A., 1996. Effects of chemical environment on dislocation creep of quartzite. Journal of Geophysical Research 101, 22143–22155.

Ruffini, R., Borghi, A., Cossio, R., Olmi, F., Vaggelli, G., 2002. Volcanic quartz growth zoning identified by Cathodoluminescence and EPMA studies. Mikrochimica Acta 139, 151–158.

Rusk, B., Sekine, K., Hirano, N., Tsuchiya, N., 2006. Insights into vein formation and alteration from experimentally synthesized hydrothermal quartz veins. In: Geological Society of America, Abstracts with Programs, vol. 38, p. 244.

Rutter, E.H., 1983. Pressure solution in nature theory and experiment. Journal of the Geological Society 140, 725–740.

Ryder, R.T., Zagorski, W.A., 2003. Nature, origin, and production characteristics of the lower Silurian regional oil and gas accumulation, central Appalachian basin, United States. American Association of Petroleum Geologists 87, 847–872.

Secor, D.T., 1965. Role of fluid pressure in jointing. American Journal of Science 263, 633–646.

Selverstone, J., 2005. Preferential embrittlement of graphitic schists during extensional unroofing in the Alps: the effect of fluid composition on rheology in low-permeability rocks. Journal of Metamorphic Geology 23, 461–470.

Selverstone, J., Holyoke, C.W., Tullis, J., 2003. Variations in quartzite rheology as a function of metamorphic fluid composition; results of coupled fluid inclusion and experimental studies. In: Geological Society of America, Abstracts with Programs, vol. 35, p. 91.

Sibley, D.F., Blatt, H., 1976. Intergranular pressure solution and cementation of the Tuscarora orthoquartzite. Journal of Sedimentary Petrology 46, 881–896.

Sibley, D.F., Vogel, T.A., Walker, B.M., Byerley, G., 1976. The origin of oscillatory zoning in plagioclase: a diffusion and growth controlled model. American Journal of Science 276, 275–284.

Sibson, R.H., 1977. Fault rocks and fault mechanisms. Journal of the Geological Society of London 133, 140–213.

Sibson, R.H., 1990. Faulting and fluid flow. In: Nesbitt, B.E. (Ed.), Short Course on Fluids in Tectonically Active Regimes of the Continental Crust 18 MAC Short Course Handbook, pp. 93–129.

Sibson, R.H., 1996. Structural permeability of fluid-driven fault-fracture meshes. Journal of Structural Geology 18, 1031–1042.

Sibson, R.H., 2001. Seismogenic framework for hydrothermal transport and ore deposition. In: Richards, J.P., Tosdal, R.M. (Eds.), Structural Controls on Ore Genesis. Reviews in Economic Geology 14, 25–50.

Sibson, R.H., Robert, F., Poulsen, K.H., 1988. High angle reverse faults, fluid pressure cycling, and mesothermal gold–quartz deposits. Geology 16, 551–555.

Sibson, R.H., Evernden, J.F., Sharp, R.V., 1979. Fluid flow around faults: field evidence for dilatancy pumping? In: U.S. Geological Survey Open-File Report 79–1239, p. 527.

Stewart, M., Holdsworth, R.E., Strachan, R.A., 2000. Deformation processes and weakening mechanisms within the frictional–viscous transition zone of major crustal-scale faults: insights from the Great Glen Fault Zone, Scotland. Journal of Structural Geology 22, 543–560.

Stipp, M., Tullis, J., Behrens, H., 2006. Effect of water on the dislocation creep microstructure and flow stress of quartz and implications for the recrystallized grain size piezometer. Journal of Geophysical Research 111, B04201.

Taylor, H.P., 1974. The application of oxygen and hydrogen isotope studies to problems of hydrothermal alteration and ore deposition. Economic Geology 69, 843–883.

Tuttle, O.F., 1949. Structural petrology of planes of liquid inclusions. Journal of Geology 57, 331–356.

van den Kerkhof, A.M., Kronz, A., Simon, A., 2001. Trace element redistribution in metamorphic quartz and fluid inclusion modification: observations by cathodoluminescence. XVI ECROFI, European Current Research on Fluid Inclusions, Porto, pp. 447–450.

van den Kerkhof, A.M., Kronz, A., Simon, K., Scherer, T., 2004. Fluid-controlled quartz recovery in granulite as revealed by cathodoluminescence and trace element analysis (Bamble sector, Norway). Contributions to Mineralogy and Petrology 146, 637–652.

Walther, J.V., 2005. Essentials of Geochemistry. Jones and Bartlett, Boston.

Wawrzyniec, T., Selverstone, J., Axen, G.J., 1999. Correlations between fluid composition and deep-seated structural style in the footwall of the Simplon low-angle normal fault, Switzerland. Geology 27, 715–718.